Available online at www.sciencedirect.com
SCIENCE DIRECT®
Mechatronics 14 (2004) 1141–1155
MECHATRONICS

A gap capacitance method for slider flying height measurement in near-field optical disk drives

J.W. Chen, T.S. Liu *

Department of Mechanical Engineering, National Chiao Tung University, Hsinchu 30010, Taiwan, ROC

Received 5 November 2003; accepted 28 June 2004

Abstract

In order to overcome the diffraction limit of conventional optical disk drives, and substantially increase data storage capacity and density, near-field optical disk drives remain to be realized. The slider of a flying pickup head in a near-field optical disk drive has to fly at a stable spacing above the disk surface. To sense the slider flying height, a gap capacitance method is developed in this study to measure capacitance variation between the pickup head and disk surface. The capacitance varying with the flying height is modulated by a Colpitts oscillator. Subsequent demodulation accounts for height variation of the flying pickup head. Measurement results of this method are verified by using a laser Doppler interferometer.

Keywords: Flying pickup head; Near-field optical disk drive; Flying height; Gap capacitance

1. Introduction

Conventional optical disk drives have a diffraction limit in optics, since its operation situation is in far-field i.e. $d \gg \lambda$; where d is the distance between a sample and a source and λ is the free space wavelength of a light source. In view of this,

* Corresponding author. Fax: +886 35720634.
E-mail address: tsliu@mail.nctu.edu.tw (T.S. Liu).

0957-4158/$ - see front matter
doi:10.1016/j.mechatronics.2004.06.008

there are two methods for increasing optical dots per inch: (1) choose the spot source with shorter wavelength; (2) let the distance between the disk and laser beam source be smaller than the wavelength. Both belong to near-field optics. Accordingly, current optical disk drives are faced with the diffraction limit, such that their data storage density can not be further increased. For the sake of next-generation ultra high-density data storage and overcoming the diffraction limit, near-field optical disk drives that apply near-field optics [1] employ a flying pickup head with a solid immersion lens [2], thereby substantially increasing data storage capacity and density. Near-field optical disk drives employs a flying pickup head that flies in a manner similar to that in hard disk drives as shown in Fig. 1. The laser spot size can be reduced according to near-field optics theory so as to substantially increase data storage capacity, since achievable bit density is determined by the laser spot size, i.e., λ/NA, where λ is the free space wavelength and NA the numerical aperture of an objective lens. The use of a solid immersion lens increases the effective numerical aperture.

However, a critical requirement in increasing areal density is the low flying head height i.e. the spacing between the flying pickup head and disk surface must be very small. The flying pickup head has to maintain a stable near-field height for focusing. In this study, to measure height variation of the flying head; i.e., head–disk gap, a gap capacitance method is developed. Experimental results are presented to demonstrate the effectiveness of the proposed method.

It has been attempted to achieve stable and small spacing between a flying pickup head and a disk surface by using passive air-bearing sliders to implement near-field recording [2,3]. It is common to use laser Doppler vibrometers for sensing optical disk flutter and flying height variation [4,5]. Although laser Doppler vibrometers are accurate in measurement, this study aims to develop an alternative approach—a gap capacitance method—that is more economical than other approaches.

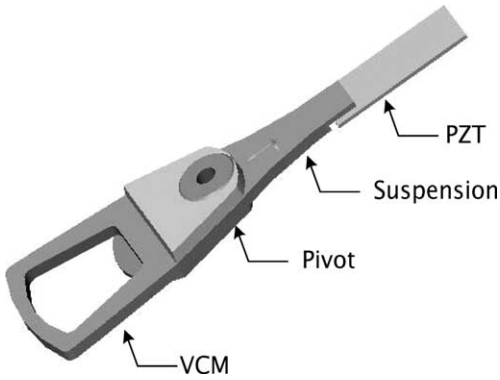

Fig. 1. Flying head design in NFODD.

2. Gap capacitance method

This study develops a gap capacitance method to measure the flying height of a pickup head. To use the gap capacitance sensor has to make the pickup head excessively close to the near-field optical disk. The proposed method can measure the varying spacing between the flying pickup head and the disk without regard to varying disk rotation speed.

The piezoelectric (PZT) elements have been widely applied to be a micro-actuator in the high data storage density disk drive development, and its response performance is qualified to deal with fast and precise movement. PZT actuators can generate rapid and fine motion for the flying pickup head, where a controller with high precision is required. Among PZT actuators, PZT benders are popular in many small structure applications, such as individual blade control of rotorcraft, vibration dampening, and positional control. In the presence of disk surface vibration, a flying head with a PZT bender is attached to a suspension arm to maintain the near-field flying height.

This study pastes a copper electrode to the bottom surface of a PZT bender, as illustrated in Fig. 2. The metal thin layer coated on an optical disk becomes another electrode, whose electric charge density is constant. Hence, the metal electrode on the PZT bender and the metal thin layer constitute a capacitor, whose capacitance varies with the head–disk gap distance. The gap capacitance is generally written as [6–8]

$$C_{\text{gap}} = \varepsilon \frac{A}{X} \tag{1}$$

where ε is a permittivity, A is the effective area of the electrode, and X is the gap between the electrode and the disk surface.

The block diagram of the GCS system is depicted in Fig. 3. The capacitance signal enters a Colpitts oscillator circuit and converts into an approximate sinusoidal signal, for which one can tune a suitable frequency. As shown in Fig. 4, a Colpitts oscillator circuit is employed in this study to convert capacitance variation into a

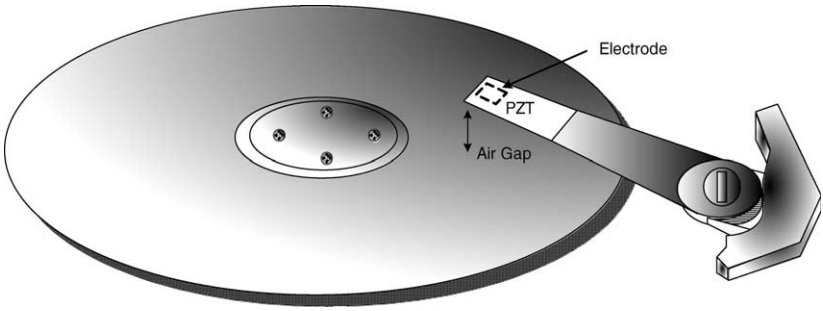

Fig. 2. Electrode and facing material as a capacitor.

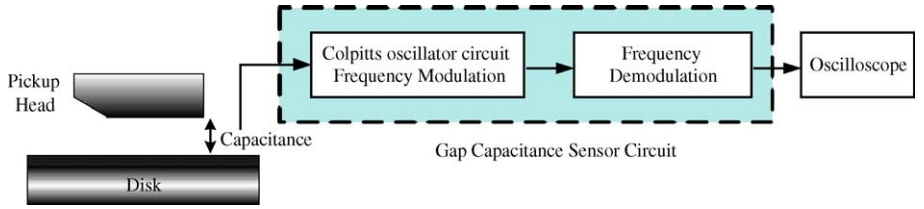

Fig. 3. Block diagram of gap capacitance sensor.

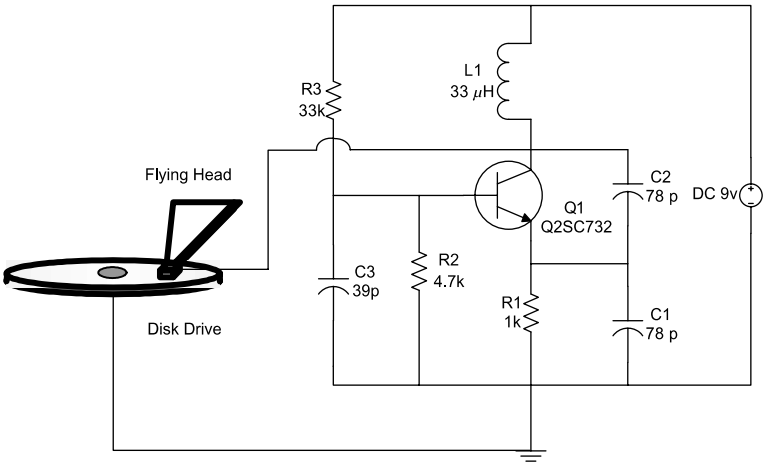

Fig. 4. Colpitts oscillator circuit.

sinusoidal carrier signal of frequency f by capacitance C_1, C_2, and inductance L_1. The carrier frequency f is expressed by [9]

$$f = \frac{1}{2\pi\sqrt{L_1\left(\frac{C_1C_2}{C_1+C_2}\right)}} \tag{2}$$

When the Colpitts oscillator circuit is parallel with a gap capacitance C_{gap}, its modulation frequency f_i becomes, based on Eq. (2),

$$f_i = \frac{1}{2\pi\sqrt{L_1\left(C_{\text{gap}} + \frac{C_1C_2}{C_1+C_2}\right)}} \tag{3}$$

Eq. (3) can be used to calculate the capacitance value C_{gap}, which depends on the flying height X according to Eq. (1). However, the frequency modulation f_i can not be measured directly in time domain. After frequency modulation (FM) by the Colpitts oscillator, an FM demodulation meter converts the modulated signal, thereby obtaining a demodulation voltage signal whose magnitude can be translated into the flying height variation.

3. Measurement

An FM signal $s(t)$ defined by

$$s(t) = A_c \cos \theta_i(t) = A_c \cos \left[2\pi f_c t + 2\pi k_f \int_0^t m(t) \mathrm{d}t \right] \tag{4}$$

is a nonlinear function of a modulating signal $m(t)$, which makes frequency modulation a nonlinear process, where f_c denotes a carrier frequency and k_f a constant. Consider the disk surface displacement in vibration as a sinusoidal modulating signal defined by

$$m(t) = A_m \cos(2\pi f_m t) \tag{5}$$

The instantaneous frequency of the resulting FM signal is written as

$$f_i(t) = f_c + k_f A_m \cos(2\pi f_m t) = f_c + \Delta f \cos(2\pi f_m t) \tag{6}$$

where $\Delta f = k_f A_m$ denotes a frequency deviation, representing the maximum departure of the instantaneous frequency of an FM signal from the carrier frequency f_c. A fundamental characteristic of FM signals is that the frequency deviation Δf is proportional to the amplitude A_m of the modulating signal and is independent of the modulating frequency. Since the instantaneous frequency of the FM signal is f_i, the FM phase can be written as

$$\theta_i(t) = 2\pi \int_0^t f_i(t) \mathrm{d}t$$

Using Eq. (6), the phase θ_i of the FM signals is obtained as

$$\theta_i(t) = 2\pi f_c t + \frac{\Delta f}{f_m} \sin(2\pi f_m t) \tag{7}$$

The ratio of the frequency deviation Δf to the modulation frequency f_m is commonly called the modulation index of the FM signal, denoted by β; i.e.

$$\beta = \frac{\Delta f}{f_m} \tag{8}$$

and Eq. (7) becomes

$$\theta_i(t) = 2\pi f_c t + \beta \sin(2\pi f_m t) \tag{9}$$

Accordingly, the parameter β in radians represents the phase deviation of the FM signal, i.e. the maximum departure of the phase $\theta_i(t)$ from the phase $2\pi f_c t$ that is the unmodulated carrier. Using Eq. (9), the FM signal in Eq. (4) can be rewritten as

$$s(t) = A_c \cos[2\pi f_c t + \beta \sin(2\pi f_m t)] \tag{10}$$

At first, the disk vibration signal enters a Colpitts oscillator circuit. The disk vibration signal 90 Hz is modulated on the carrier signal. Fig. 5 depicts a resulting carrier signal shown on the oscilloscope, where the oscillation frequency is at 4.42 MHz. In Eq. (3), $L_1 = 33$ μH and $C_1 = C_2 = 78$ pF, hence $f = 4.436$ MHz. If $C_{\mathrm{gap}} = 10$ pF,

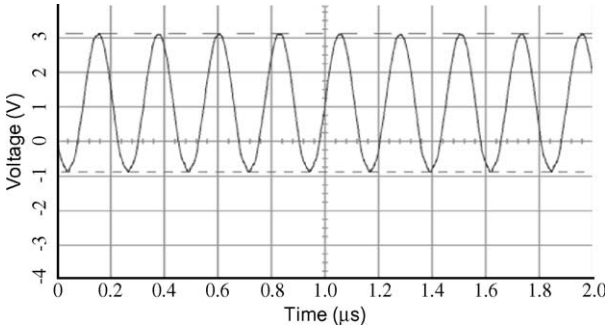

Fig. 5. Measured signal of Colpitts oscillator.

$f = 3.958$ MHz. After modulation, the carrier frequency signal reduces from 4.42 to 3.958 MHz which is an FM signal. The frequency response of disk modulation signal on the oscilloscope is shown in Fig. 6, where the resonance at $f = 3.958$ MHz comes from carrier signals in the Colpitts oscillator and the frequency deviation about 0.46 MHz is caused by C_{gap} that varies with disk rotating at 90 Hz.

This study investigates gap capacitance dealing with three disks. The first disk tested has a polycarbonate substrate and has been aluminum-coated beforehand to enhance measurement signal. When the disk does not rotate, the demodulation signal remains zero, as shown in Fig. 7. During disk rotation, the demodulation signal is shown in Fig. 8, where jerks arise from scratches on the tested disk surface.

The second disk is chromium-coated with a polycarbonate substrate and its demodulation signal is shown in Fig. 9. The third is essentially a glass-substrate disk, whose resulting demodulation signal is shown in Fig. 10. Fig. 11 compares frequency spectrums between idle and rotating disks. It is observed that the fundamental frequency of idle and rotating signals are 60 and 90 Hz, respectively. The idle signals of 60 Hz and its multiple frequencies are caused by a power source. Comparing Figs.

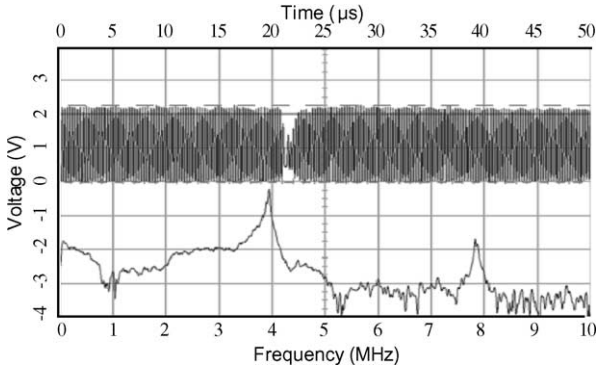

Fig. 6. FFT of modulation signal.

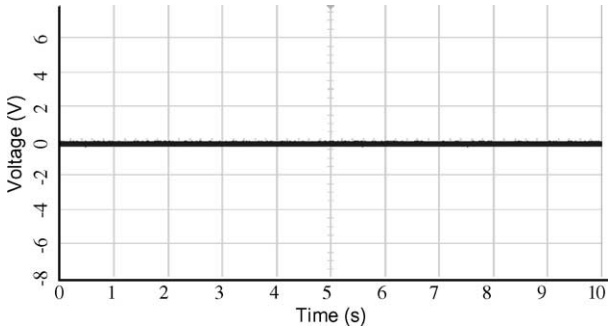

Fig. 7. Demodulation signal of aluminum-coated disk at 0 rpm.

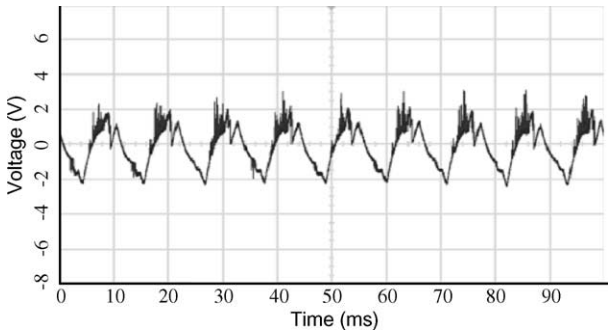

Fig. 8. Demodulation signal of aluminum-coated disk at 5400 rpm.

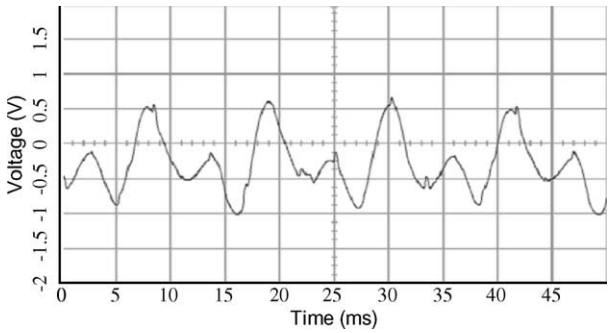

Fig. 9. Demodulation signal of chromium-coating disk at 5400 rpm.

9–11 shows that the disk substrate material dominates vibration behavior of disks. A stiffer disk yields smoother signals.

Finally, disk vibration and the capacitance gap between the electrode and disk are measured by a laser Doppler vibrometer (LDV) whose resolution is 0.2 nm, finer than a GCS. The single-beam LDV measures vibration of the chromium-coating

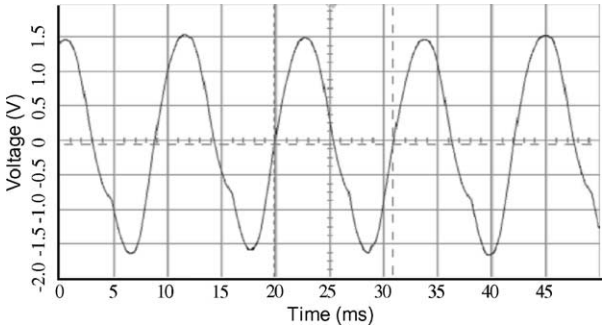

Fig. 10. Demodulation signal of glass-substrate disk at 5400 rpm.

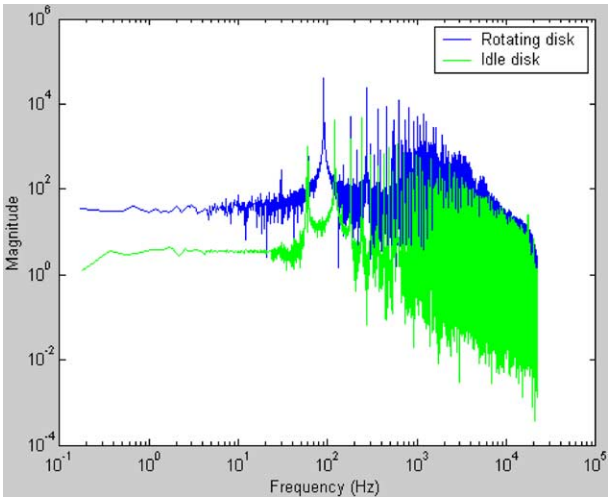

Fig. 11. Comparison of frequency spectrums between idle and rotating disks.

disk rotating at 5400 rpm is shown in Fig. 12, where the dominant frequency of the disk vibration is 88.97 Hz synchronous with the spindle motor speed and the peak-to-peak amplitude is 44.34 μm. By contrast, the measurement result for a glass-substrate optical disk is shown in Fig. 13, where the dominant frequency of the disk vibration is 89.75 Hz synchronous with the spindle motor and the peak-to-peak amplitude is 37.87 μm. Accordingly, the glass-substrate disk generates smaller deformation due to its larger hardness. Furthermore, using a dual-beam LDV, the measurement result of the gap between the electrode and the chromium-coated disk is shown in Fig. 14, where the resonant frequency is 89.84 Hz and the peak-to-peak amplitude is 92.32 μm. In addition, the dual-beam LDV is also employed to measure the gap between the electrode on a PZT bender and a glass-substrate optical disk as shown in Fig. 15, where the vibration frequency is 89.96 Hz and the magnitude of peak-to-peak is 38.82 μm. Comparing Figs. 9 and 14 yield a relationship between

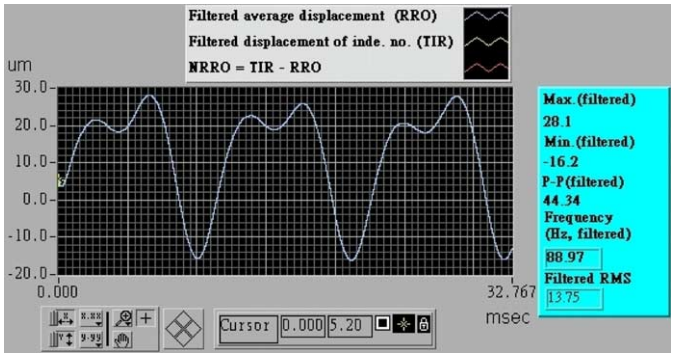

Fig. 12. Measured result by single beam LDV for optical disk with chromium coating.

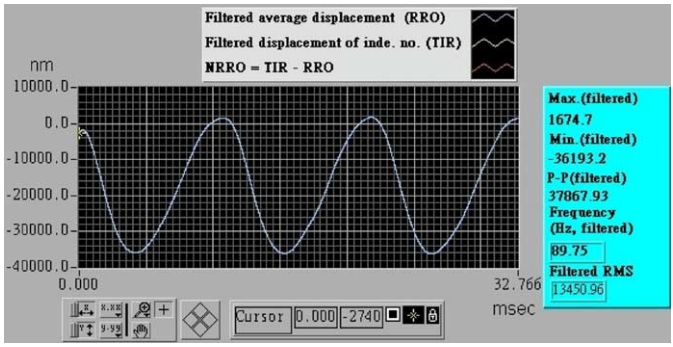

Fig. 13. Measured result by single beam LDV for glass-substrate optical disk.

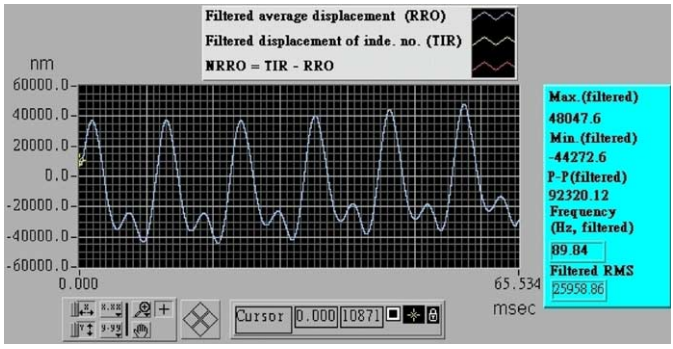

Fig. 14. Flying height variation measured by dual-beam LDV for chromium-coating optical disk.

the demodulated voltage and capacitance gap as 1.0 V = 57.7 μm for the chromium coating disk. By contrast, Fig. 16 yields the relationship between voltage and capacitance gap as 1.0 V = 12.4 μm for the glass-substrate disk. The curves for flying

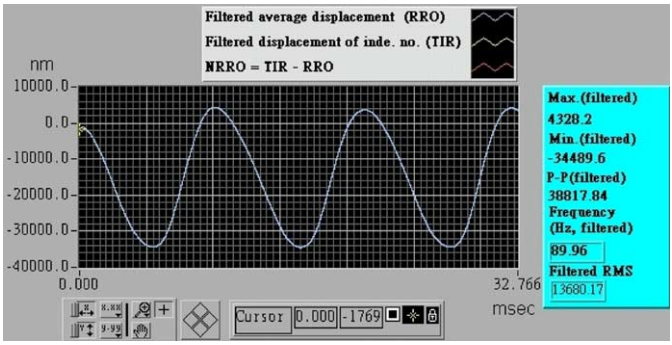

Fig. 15. Flying height variation measured by dual-beam LDV for glass-substrate optical disk.

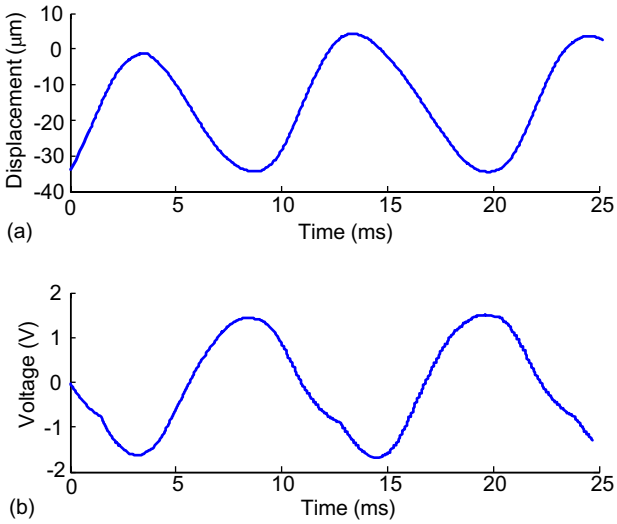

Fig. 16. Comparison of flying height curve (a) in Fig. 15 and demodulation signal (b) obtained from GCS.

height and demodulated voltage are out of phase, since according to Eq. (1) flying higher correspond to smaller capacitance and hence smaller demodulated voltage. Fig. 16(a) resulting from LDV measurement validates the proposed gap capacitance method that yields Fig. 16(b).

4. Electrode and gap capacitance

Fig. 17 shows capacitance values vs. air gap in measurement, where dots are obtained by capacitance meter measurement in static state. The regression curve in Fig. 17 can be expressed by

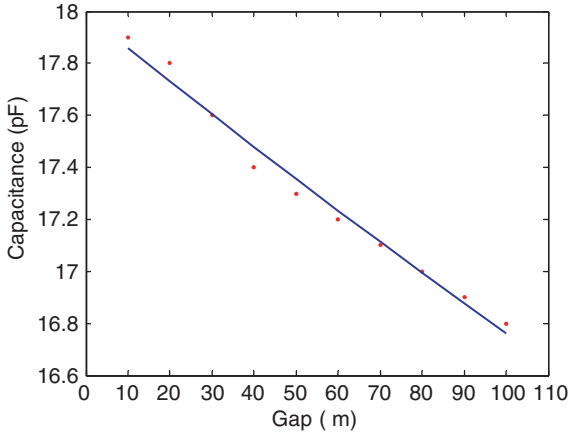

Fig. 17. Capacitance values vs. air gap in static state.

$$C = \frac{24534.82}{X + 1363.79} \tag{11}$$

where X is the distance in μm between the disk and pickup head. Eq. (11) is similar to Eq. (1) other than the appearance of a constant term in the denominator. Denoting C_{gap} and C_p as measured gap capacitance and parasitic capacitance, respectively, the equivalent capacitance of two capacitors in series is written as

$$C = \frac{1}{\frac{1}{C_{gap}} + \frac{1}{C_p}} \tag{12}$$

Substituting Eq. (1) into (12) yields

$$C = \frac{1}{\frac{1}{\varepsilon\frac{A}{X}} + \frac{1}{C_p}} = \frac{\varepsilon A}{X + \frac{\varepsilon A}{C_p}} \tag{13}$$

Comparing Eq. (11) with (13) leads to $\varepsilon A = 24534.82$ and $C_p = 18$ pF. Hence, the present experimental data consists with the general model, i.e. Eq. (1).

Eq. (12) can also be rewritten as

$$C = \frac{C_{gap}C_p}{C_{gap} + C_p} \tag{14}$$

Accordingly, if C_{gap} is much larger than C_p, then $C \fallingdotseq \frac{C_{gap}C_p}{C_{gap}} = C_p$ such that the gap capacitance effect is not apparent. If $C_{gap} \fallingdotseq C_p$, then Eq. (14) yields $C \fallingdotseq \frac{C_{gap}^2}{2C_{gap}} = C_{gap}/2$. By contrast, if C_{gap} is much smaller than C_p, then $C \fallingdotseq \frac{C_{gap}C_p}{C_p} = C_{gap}$. Therefore, a too large gap capacitance is not amenable to gap capacitance measurement. Moreover, a smaller C_{gap} i.e. smaller size electrode is essential. A smaller size electrode can produce more uniform capacitance distribution on a measured surface.

Since the larger electrode and disk surfaces do not remain parallel during disk rotation, measured capacitance voltages are not accurate. To avoid this problem should make the electrode as small as possible. The capacitance of a small electrode can be treated as uniform distribution. The measured area on a disk will be small, by which measurement accuracy can be improved.

5. Simulation results

This study carries out control simulation with an identified model of a PZT bender and uses measured vibration data of an optical disk to demonstrate the effectiveness of the gap capacitance sensing method. By using system identification, a PZT bender transfer function that relates control voltage U (volt) to bender vertical displacement Y (μm) is written as

$$\begin{aligned}\mathrm{PZT}(s) &= \frac{Y(s)}{U(s)} \\ &= \frac{1.735\times 10^{8}s^{2} + 2.094\times 10^{10}s + 1.844\times 10^{15}}{s^{4} + 1231s^{3} + 1.03\times 10^{8}s^{2} + 2.547\times 10^{10}s + 4.142\times 10^{14}}\end{aligned} \tag{15}$$

To suppress variation of the head/disk spacing, the optical pickup head is demanded to track disk deformation in the focusing direction. Fig. 18 illustrates the block diagram for the present control system, in which $D(s)$ minus PZT(s) output becomes the flying height error to be minimized. Considering a PZT model without disturbance and system uncertainty, this study designs a controller expressed by

$$C(s) = \frac{130s + (2\pi 90)^{2}}{s^{2} + (2\pi 90)^{2}} \tag{16}$$

which aims to deal with 90 Hz vibratory deformation of a disk surface. As depicted in Fig. 18, the error can be written as

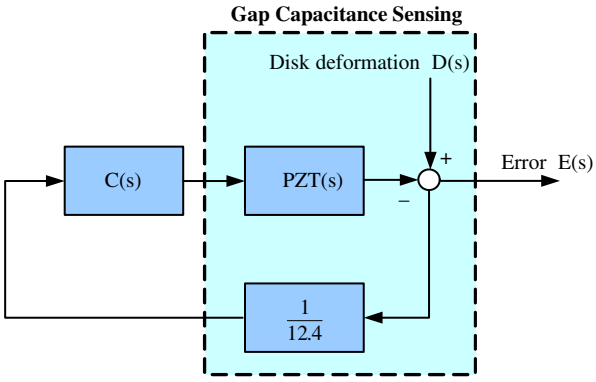

Fig. 18. Block diagram in control simulation.

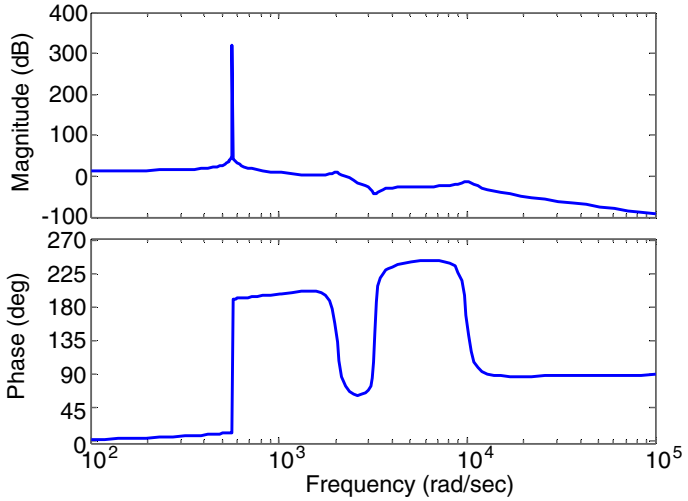

Fig. 19. Bode diagram of open loop system.

$$E(s) = \frac{12.4}{12.4 + \mathrm{PZT}(s)C(s)} D(s) \tag{17}$$

where 12.4 is the gain of a gap capacitance sensor from displacement to voltage and $D(s)$ denotes disk surface deformation. Eq. (15) multiplied by (16) yields the Bode diagram of the open loop gain as shown in Fig. 19, which shows remarkably high

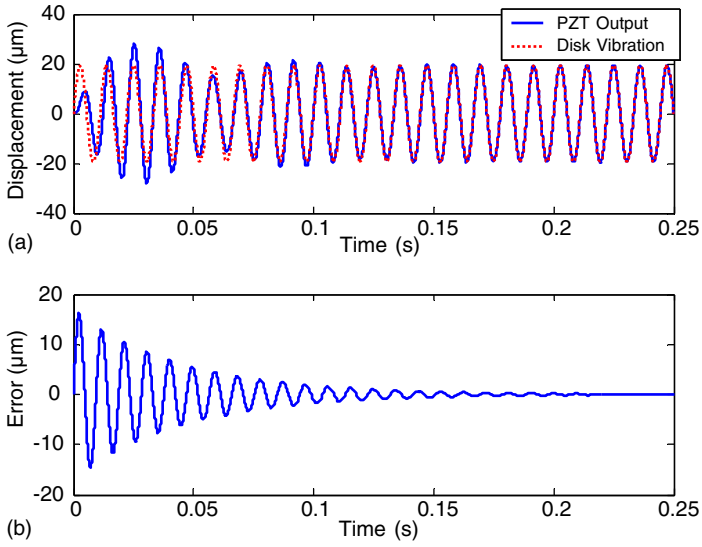

Fig. 20. Simulation result of flying height control.

gain at 90 Hz. The flying height disturbance due to disk vibration at 90 Hz can thus be eliminated by this control method. Fig. 20(a) depicts simulation results of flying height control, where the dotted curve as reference input represents the vibration of a near field glass-substrate disk, while the solid curve is the PZT bender displacement. Based on Eq. (17), Fig. 20(b) depicts the error in Fig. 20(a). The result shows that stable flying height is achieved. Nevertheless, to carry out gap capacitance sensing in practice, discharge arc between electrodes may occur, which is to be avoided. To this end, the circuit in Fig. 4 has to be modified.

6. Conclusion

Gap capacitance sensor accuracy has been verified by the measurement result of a dual-beam LDV. Hence, the proposed sensing method is validated. For the flying pickup head in near-field optical disks, this study develops a gap capacitance method for position sensing. In experiments, the gap capacitance sensor has been used to measure head flying heights above polycarbonate-substrate and glass-substrate disks, respectively. In the present gap capacitance sensing method, the varying spacing between flying pickup head and disk surface can be detected by frequency modulation and demodulation. Experimental results yield gains 1.0 V = 57.7 μm for a polycarbonate-substrate optical disk and 1.0 V = 12.44 μm for a glass-substrate optical disk. Therefore, polycarbonate-substrate optical disks indeed deform more severe than glass-substrate optical disks. The flying height and demodulated voltage are out of phase. It is seen that measurements results obtained by both gap capacitance sensor and LDV are consistent. Although GCS is much cheaper than LDV, its drawbacks include high output noise and uneven capacitance distribution, which can be improved by designing a high performance oscillator circuit and a smaller electrode.

Acknowledgments

This work was supported by Department of Education in Taiwan, Republic of China under Grant No. 89E-FA06-1-4.

References

[1] Betzig E, Trautman JK, Wolfe R, Gyorgy EM, Finn PL, Kryder MH et al. Near-field magneto-optics and high density data storage. Appl Phys Lett 1992;61(2):142–4.
[2] Ichimura I, Hayashi S, Kino GS. High-density optical recording using a solid immersion lens. Appl Optics 1997;36(19):4339–48.
[3] Hasegawa S, Aoyama N, Futamata A, Uchiyama T. Optical tunneling effect calculation of a solid immersion lens for use in optical disk memory. Appl Optics 1999;38(11):2297–300.
[4] Zeng QH, Thornton BH, Bogy DB, Bhatia SC. Flyability and flying height modulation measurement of sliders with sub-10 nm flying heights. IEEE Trans Magnetics 2001;37(2):894–9.

[5] Tanaka H, Yonemura S, Tokisue H. Slider dynamics during continuous contact with textured and smooth disks in ultra low flying height. IEEE Trans Magnetics 2001;37(2):906–11.
[6] Giancoli DC. Physics for scientists and engineers with modern physics. Prentice-Hall; 1988.
[7] De Silva CW. Control sensors and actuators. Prentice-Hall; 1989. p. 113–6.
[8] Zhao W, He N, Cao G. A microcomputer-controlled scanning Fabry-Perot interferometer. In: SPIE Conference on Optomechanical Design and Engineering Denver, Colorado, July 1999, vol. 3786. p. 515–22.
[9] Sedra AS, Smith KC. Microelectronic circuits. Saunders College Publishing; 1991.